Supplementary Materials for
Weak Topological Insulators and Composite Weyl Semimetals: β-Bi4X4 (X=Br, I)

Cheng-Cheng Liu, Jin-Jian Zhou, Yugui Yao, and Fan Zhang

Contents

A. Computational methods

Our DFT calculations are performed using the projector augmented wave method implemented in the Vienna *ab initio* simulation package (VASP) [1]. Perdew-Burke-Ernzerhof parametrization of the generalized gradient approximation (GGA-PBE) is used for the exchange correlation potential [2, 3]. The plane wave energy cutoff is set to 300 eV, and the Brillouin zone is sampled by a $9 \times 9 \times 6$ mesh. Based on the experimental or the optimized lattice structures, we apply the more sophisticated and accurate Heyd-Scuseria-Ernzerhof (HSE) hybrid functional method [4] to the calculations of electronic band structures, using a 300 eV wave energy cutoff and a $6 \times 6 \times 4$ Brillouin zone mesh.

In studying the surface states, we first use the bulk DFT results and the Wannier90 code [5–7] to construct the maximally localized Wannier functions for the p orbitals of Bi and halogens. Based on the Wannier functions, we then use an iterative method [8] to obtain the surface Green's functions of semi-infinite systems, from which we calculate the dispersions of surface states.

Under strain, the atomic positions are allowed to be optimized until the force on every ion is less than 0.01 eV/Å by employing the vdW corrections [9, 10]. Since β-Bi_4Br_4 has yet to be synthesized in experiment, we calculate the phonon spectrum to investigate its lattice stability, using the PHONOPY code [11]. The vdW corrections and lattice relaxations are also employed to obtain the optimized atomic positions and lattice parameters for β-Bi_4Br_4, which are list in Table I.

B. Topologically trivial electronic band structure of α-Bi_4X_4 (X=I, Br)

We employ the HSE hybrid functional method [4], which is believed to be more sophisticated and accurate than the GGA and LDA methods, to carry out our density functional theory (DFT) calculations of the electronic band structures of α-Bi_4I_4 and α-Bi_4Br_4 [12–15], including the spin orbital couplings (SOC). More details on the calculations can be found in *Computational Methods* in the main text. Figure 1 shows the bulk band structures of α-Bi_4I_4 and α-Bi_4Br_4. Clearly, in both α-phase materials the energy bands around the Fermi levels are mainly contributed by Bi p_x-orbitals, similar to their β-phase cousins. By comparing the Fig. 1 here and the Fig. 2 in the main text, we find that the valence and conduction bands are inverted twice at both L and M points in both α-phase materials. Therefore, based on the Fu-Kane criterion [16] α-Bi_4I_4 and α-Bi_4Br_4 are both trivial insulators, with gaps of 40 meV and 145 meV, respectively. This conclusion has been further confirmed by our direct calculations of the Z_2 index.

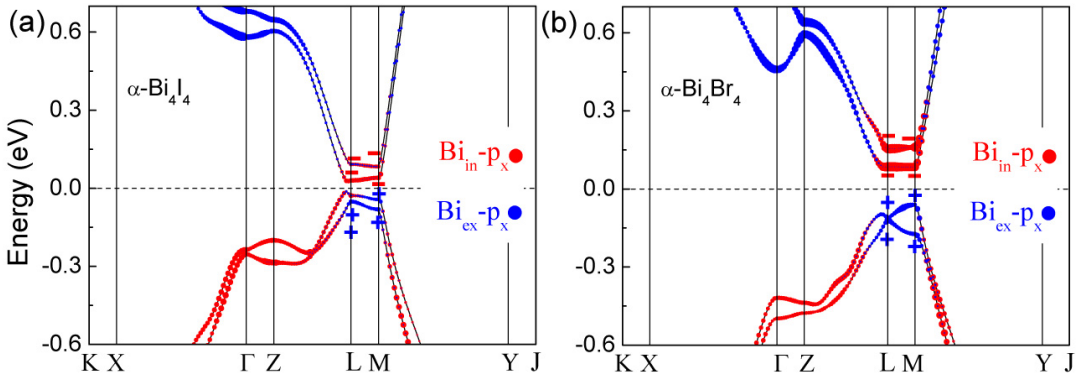

FIG. 1: The bulk electronic band structures of (a) α-Bi_4I_4 and (b) α-Bi_4Br_4, where SOC are included and HSE are employed. The size of red (blue) dots indicates the weight of the relevant p_x orbital of Bi_{in} (Bi_{ex}) atoms. The symbols + and − label the parity eigenvalues of the band edges at L and M points. The dashed lines indicate Fermi levels.

C. Phonon spectrum and crystal structure of β-Bi_4Br_4

Bulk Bi_4X_4 (X=Br, I) have both α and β phases. α-Bi_4I_4, β-Bi_4I_4, and α-Bi_4Br_4 have been experimentally synthesized before [12–15]. Here we demonstrate that β-Bi_4Br_4 should also be a stable phase by calculating its phonon spectrum. To pursue the most accurate structure of β-Bi_4Br_4, we take into account the van der Waals (vdW) corrections and the relaxation of lattice constants and atomic positions in our DFT calculations. More details on the calculations can be found in *Computational Methods* in the main text. The optimized crystal structure and atomic positions of β-Bi_4Br_4 are summarized in Table I.

TABLE I: DFT+vdW relaxed crystal structure and atomic positons of β-Bi_4Br_4.

Material	Space group	Crystal structure	Atomic Positons: x y z
β-Bi_4Br_4	C_{2h}^3 (C2/m)	a= 6.998 Å , b=6.998 Å , c=10.191 Å ; $\alpha = 106.96°, \beta = 106.96°, \gamma = 36.11°$	Bi1 0.8323 0.8323 0.0108
			Bi2 0.1677 0.1677 0.9892
			Bi3 0.2103 0.2103 0.3025
			Bi4 0.7897 0.7897 0.6975
			Br1 0.5533 0.5533 0.2461
			Br2 0.4467 0.4467 0.7539
			Br3 0.8672 0.8672 0.3734
			Br4 0.1328 0.1328 0.6266

We further calculate the phonon spectrum of β-Bi_4Br_4, as seen in Fig. 2. Clearly, there is no imaginary frequency in the whole Brillouin zone, indicating that the optimized β-Bi_4Br_4 is a stable structure.

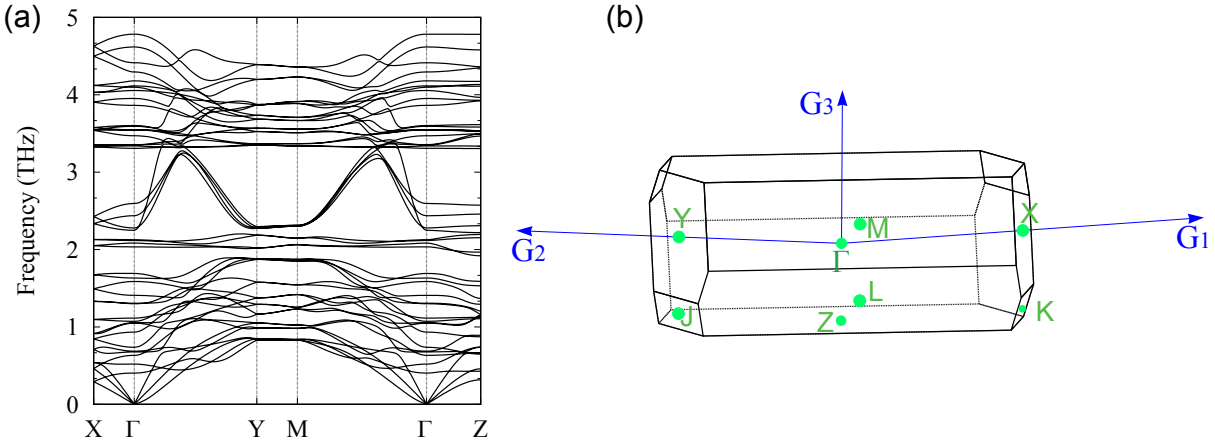

FIG. 2: (a) Phonon spectrum of β-Bi_4Br_4. (b) The Brillouin zone of β-Bi_4Br_4.

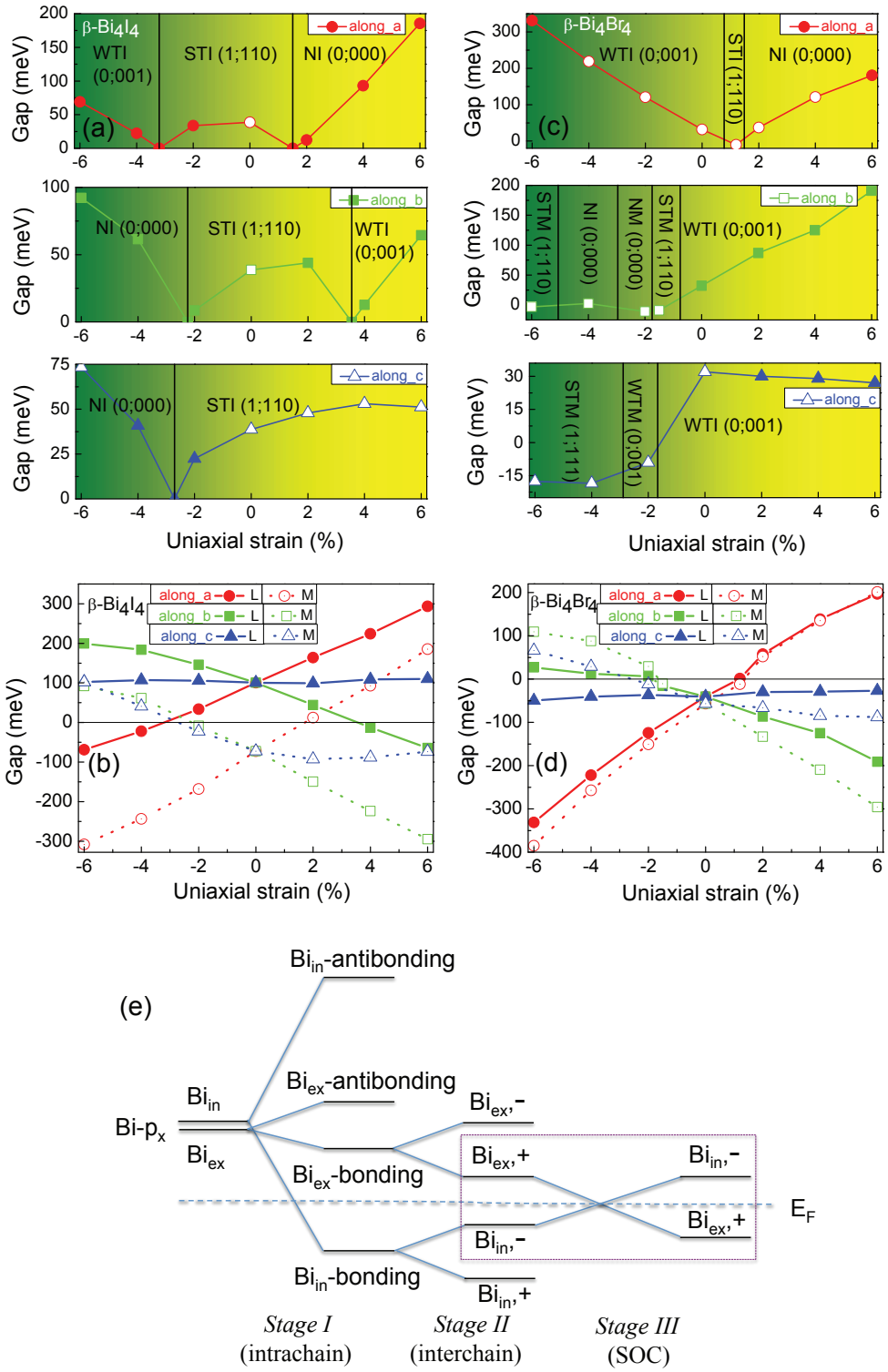

FIG. 3: (a) Topological phase diagrams and direct band gaps at L and M points under uniaxial strain along $\boldsymbol{a}$, $\boldsymbol{b}$, and $\boldsymbol{c}$ axes. (a) and (b) for β-Bi_4I_4; (c) and (d) for β-Bi_4Br_4. A solid (open) symbol denotes a direct (indirect) gap. (e) Schematic diagram of the band evolution at L and M points; the detailed evolutions are explained in the text.

D. Topological quantum phase transitons under uniaxial strain

α- and β-Bi_4X_4 (X=I, Br) can be considered as a periodic stack of one dimensional atomic chains which are the building blocks [12–15]. It follows that these materials are anticipated to respond differently to uniaxial strain along and perpendicular to the atomic chains. We consider three types of uniaxial strain in the two β-phases, i.e., along the atomic chain (in the $\boldsymbol{b}$ direction) and perpendicular to the chain (in the $\boldsymbol{a}$ and $\boldsymbol{c}$ directions). As shown in Fig. 3(a)-(d), the application of uniaxial strain in each direction can effectively engineer the band gaps at M and L points, which can induce quantum phase transitions among the three topologically distinct phases: strong topological insulator (STI), weak topological insulator (WTI), and normal insulator (NI). Since the spatial inversion symmetry can not be broken by strain for the reason that we have given in the main text, the Weyl semimetal phase does not appear in the phase diagrams.

For example, β-Bi_4I_4 is a STI without strain, with the only band inversion at M point. Under tensile strain along the $\boldsymbol{b}$ axis, the gap at L could become inverted while the gap at M remains inverted, driving β-Bi_4I_4 from a STI to a WTI. On the other hand, under compressive strain, the original inverted gap at M could become un-inverted, driving β-Bi_4I_4 from a STI to a NI. In general, β-Bi_4I_4 responses inversely to strain along the $\boldsymbol{a}$ axis, compared to the responses to strain along the $\boldsymbol{b}$ and $\boldsymbol{c}$ axes. The WTI β-Bi_4Br_4 has rather similar strain responses. For β-Bi_4Br_4 under some strain rates, there are no indirect band gaps, although there exist well defined direct band gaps throughout the whole Brillouin zone. For these special cases, we use M standing for *metal* instead of I denoting *insulator* in the following abbreviations: STM, WTM, and NM.

To better understanding the physical mechanism of the band inversion and the responses of direct band gaps to strain, we take β-Bi_4I_4 for example to analyze the evolution of electronic band structure in the neighborhood of Fermi level. The main results are summarized schematically in Fig. 3(e). Due to the much larger electronegativity of halogen, the orbitals of Bi atoms are left near the Fermi level. Because the mirror plane is perpendicular to the $\boldsymbol{b}$ axis, the p_y orbitals of Bi atoms are decoupled from their p_z and p_x orbitals for the spinless case. The fact that the three internal zigzag atomic chains of one building block are displaced along the $\boldsymbol{c}$ direction gives rise to the decoupling between the p_z and p_x orbitals. From the projected band structure, we find that the p_x orbitals of Bi atoms dominate near the Fermi level. At the first stage, we take into account the more tighter intra-chain couplings that are mainly related to physics in the $\boldsymbol{b}$ direction, shown as *Stage I* in Fig. 3(e). The level splitting of the internal zigzag chain atoms Bi_{in} between the bonding and anti-bonding states turn out to be much larger than that of external atoms Bi_{ex}. At the second stage, we consider the inter-chain couplings of Bi_{in} atoms that are mainly along the $\boldsymbol{a}$ direction. Since the spatial inversion symmetry relates two chains, the energy bands can be labeled by their parity eigenvalues $\pm$, plotted as *Stage II* in Fig. 3(e). At the final stage, we turn on the SOC with the total angular momentum conserved. As a result, the $Bi^{p_x}_{in/ex,\pm}$ orbitals are mixed with the $Bi^{p_y}_{in/ex,\pm}$ ($Bi^{p_z}_{in/ex,\pm}$) orbitals that have the opposite (same) electron spin and the same parity eigenvalue. Consequently, the ordering of $Bi^{p_x}_{in,\pm}$ orbitals is inverted at M or/and L points, marked by the dashed box in Fig. 3(e). Similar analyses can be carried out for the β-Bi_4Br_4 case.

Nevertheless, because the uniaxial strains along **b** (along the atomic chain) and **a** (between the atomic chains) axes play the most significant roles at *Stage I* and *Stage II*, respectively, the band gaps must response strongly. Because during *Stage I* and *Stage II* the most relevant bands move in the relatively opposite manners, as seen in Fig. 3(e), the substantial responses to strain along $\boldsymbol{a}$ and to strain along $\boldsymbol{b}$ must exhibit the opposite signs. In contrast, there is little response to strain along the $\boldsymbol{c}$ axis, because the inter-chain couplings have a much longer distance and thus weaker strength along the $\boldsymbol{c}$ axis. These analyses, together with the effective theory and the corresponding linear dependence of direct gaps on the strain rates that are discussed in the main text, fully explain our results based on DFT calculations. We note by passing that topological quantum phase transitions would also occur in the α-phases under uniaxial strain, though the unstrained phases are boring NI.

E. Mirror Chern numbers of β-Bi_4I_4 and β-Bi_4Br_4

One may wonder whether β-Bi_4I_4 and β-Bi_4Br_4 are topological crystalline insulators (TCI) [17], since a (010) mirror symmetry is present. In a mirror invariant plane, the two spin subspaces, related by $\mathcal{T}$ symmetry, decouple and have opposite Chern numbers $\pm N$. There must be N pairs of protected Fermi points in the mirror invariant line (MIL) at the surface, independent of the Fermi level. Similar to Bi_2Se_3 [18], the STI β-Bi_4I_4 is also a TCI ($N = 1$), because there are always two surface-state Fermi points in the MIL $\bar{G}\bar{X}$, as shown in Fig. 2(c) of the main text. In contrast, the WTI β-Bi_4Br_4 is not a TCI ($N = 0$), because Fermi points are not necessarily present along the MIL $\bar{G}\bar{A}$, as seen in Figs.2(f) and 2(g) of the main text. These arguments are consistent with our direct calculations on the mirror Chern numbers [19].

[1] G. Kresse and J. Furthmüller, Phys. Rev. B **54**, 11169 (1996).
[2] J. P. Perdew, K. Burke, and M. Ernzerhof, Phys. Rev. Lett. **77**, 3865 (1996).
[3] G. Kresse and D. Joubert, Phys. Rev. B **59** 1758 (1999).
[4] J. Heyd, G. E. Scuseria, and M. J. Ernzerhof, Chem. Phys. **118**, 8207 (2003).
[5] A. Mostofi, J. R. Yates, Y.-S. Lee, I. Souza, D. Vanderbilt, and N. Marzari, Comput. Phys. Commun. **178**, 685 (2008).
[6] N. Marzari and D. Vanderbilt, Phys. Rev. B **56**, 12847 (1997).
[7] I. Souza, N. Marzari, and D. Vanderbilt, Phys. Rev. B **65**, 035109 (2001).
[8] M. P. L. Sancho, J. M. L. Sancho, and J. Rubio, J. Phys. F: Met. Phys. **15**, 851 (1985).
[9] M. Dion, H. Rydberg, E. Schroder, D. C. Langreth, and B. I. Lundqvist, Phys. Rev. Lett. **92**, 246401 (2004).
[10] J. Klimes, D. R. Bowler, and A. Michaelides, Phys. Rev. B **83**, 195131 (2011).
[11] A. Togo, F. Oba, and I. Tanaka, Phys. Rev. B **78**, 134106 (2008).
[12] H. G. von Schnering, H. von Benda, and C. Kalveram, Z. Anorg. Allg. Chem. **438**, 37 (1978).
[13] H. von Benda, A. Simon, and W. Bauhofer, Z. Anorg. Allg. Chem. **438**, 53 (1978).
[14] E. V. Dikarev, B. A. Popovkin, A. V. Shevelkov, Russ. Chem. Bull. Int. Ed. **50**, 2304 (2001).
[15] T. G. Filatovaa, P. V. Gurinb, L. Klooc, V. A. Kulbachinskiib, A. N. Kuznetsova, V. G. Kytinb, M. Lindsjoc, and B. A. Popovkina, J. Solid State Chem. **180**, 1103 (2007).
[16] L. Fu, and C. L. Kane, Phys. Rev. B **76**, 045302 (2007).
[17] T. H. Hsieh, H. Lin, J. Liu, W. Duan, A. Bansil, and L. Fu, Nat. Commun. 3, 982 (2012).
[18] F. Zhang, X. Li, J. Feng, C. L. Kane, and E. J. Mele, arXiv:1309.7682 (2013).
[19] J. C. Y. Teo, L. Fu, and C. L. Kane, Phys. Rev. B **78**, 045426 (2008).